Microfluid Nanofluid (2013) 15:509–518
DOI 10.1007/s10404-013-1170-4

RESEARCH PAPER

Fabrication of sealed nanofluidic channels using site-selective direct write (maskless) X-ray lithography

Adam F. G. Leontowich · Adam P. Hitchcock

Received: 2 December 2012 / Accepted: 4 March 2013 / Published online: 23 March 2013

Abstract Sealed nanofluidic channels with cross-sections as small as 60 nm × 60 nm were created in polymer bilayers using the focused X-rays of a scanning transmission X-ray microscope. These structures were then characterized by near-edge X-ray absorption fine structure spectromicroscopy, atomic force microscopy and scanning electron microscopy. The cross-sectional area of the nanochannels could be tuned by adjusting the area patterned in *x* and *y* and/or manipulating the bottom layer thickness. The maximum length was found to be limited by the efficiency of excavation of patterned material out of the channel, and the stability of the polymer overlayer which seals the channel. Schemes toward interfacing these nanochannels with conventional microfluidics are discussed.

Keywords STXM · Zone plate · Nanolithography · PMGI · NEXAFS

1 Introduction

Focused X-rays offer the possibility of direct write (maskless) lithography, analogous to lithography with a focused electron beam. Historically, the majority of this work has been performed using scanning transmission X-ray microscopes (STXM) operating at soft X-ray photon energies (100–2,500 eV, $\lambda = 12$–0.5 nm). The pioneering work of Zhang et al. (1995) reported feature sizes of 300 nm in poly(methyl methacrylate) (PMMA), created using the Stony Brook STXM at the National Synchrotron Light Source. Recently, Leontowich et al. (2013) working at 1 keV ($\lambda = 1.24$ nm) were able to achieve 20–25 nm lines in PMMA. The minimum feature size obtainable by direct write X-ray lithography is steadily approaching that of state-of-the-art focused ion [10 nm (Winston et al. 2009)] or electron [4.5 nm (Yang et al. 2009)] beams, which have been extensively used to fabricate micro- and nano-fluidic devices either directly or indirectly.

Patterning with monochromatic X-rays and full control over the photon energy has opened up a novel technique capable of patterning buried layers of material termed "chemically selective patterning". The concept is as follows: different molecules containing different chemical functional groups have different X-ray absorption spectra. Most resist-type molecules are polymers which experience chemical changes ("radiation damage") when irradiated (Coffey et al. 2002; Wang et al. 2009a, b). If the X-ray beam is tuned to a photon energy corresponding to an absorption resonance exclusive to one layered component, then one can induce a chemical change to that component nearly independently of the other components present at the same point in the sample. Using the Advanced Light Source (ALS) STXM 5.3.2.2, Wang et al. demonstrated that buried polymer layers can be selectively patterned in bilayer (Wang et al. 2007a) and trilayer (Wang et al. 2007b) samples.

Here, this concept is taken another step further and also directed towards a new area of application. The X-rays from a STXM were used to chemically selectively pattern a conduit in a polymer layer buried under another different polymer layer. Then, the patterned/damaged material of the buried layer was excavated using wet chemistry, leaving

A. F. G. Leontowich · A. P. Hitchcock
Brockhouse Institute for Materials Research,
McMaster University, Hamilton, ON L8S 4M1, Canada

A. F. G. Leontowich (✉)
Center for Free-Electron Laser Science,
Notkestraße 85, Hamburg 22607, Germany
e-mail: adam.leontowich@cfel.de

behind a hollow channel. Parts of this work have been presented earlier in a conference proceeding (Leontowich and Hitchcock 2012a). The dimensions of the channels fabricated in this manner are very controllable and can be in the sub-100 nm range. In addition, the channels are created in a sealed form. This is in contrast to more established nanochannel fabrication methods which involve a channel-sealing step. Examples of that approach include; etching a trench into a flat substrate such as glass, and then bonding a flat cover piece overtop (Stavis et al. 2005); or moulding features in a soft polymer stamp which is then pressed in contact with a flat substrate (Park et al. 2009). For these methods, the yield and stability of the fluidic channels is highly dependent on the quality of the bonding of the two surfaces. Channel-sealing procedures often put restrictions on the allowed arrangements and dimensions of nanochannels (Fouad et al. 2010). Channels made using direct write X-ray lithography avoid these sealing issues. In addition to fabricating channels, the underlying mechanisms of nanochannel formation were investigated and are discussed. The design rules and restrictions inherent in this technique were also investigated and are outlined here. A prototype nanofluidic device is presented, and schemes to interface such devices with conventional microfluidics to realize fully functional fluidic devices are described.

2 Methodology

2.1 Appropriate materials for chemically selective lithography

2.1.1 Controlling the location of energy absorption by chemically selective patterning

There are several sample requirements for chemically selective patterning. The foremost is that the sample must contain at least two chemically different components, and each component must have significantly different X-ray absorption spectral features. Ideally, the spectrum of each component should have a large inner shell (core electron) resonance at a chosen absorption edge, and these resonances should be separated in energy by more than their feature width, i.e., by about 0.7 eV or more. The absorption edge must also be within the energy range achievable by the beamline (80–2,500 eV for existing soft X-ray STXM beamlines; 250–750 eV for ALS STXM 5.3.2.2 where this work was performed). When patterning, the rate of energy absorption by one component can then be significantly greater than that of the other component(s) by tuning the photon energy to those specific resonance energies. In principle, the components could be selected based on different elemental composition, i.e., one component could contain F but not N, while the other contains N but not F. In practice, patterning at one absorption edge is preferred as moving between absorption edges often requires re-optimization of the STXM and beamline which may compromise the positional alignment of multiple patterns. In addition, higher energy edges such as the N, O and F 1s edges have a significant underlying absorption from the C 1s ionization continuum which is common to all molecules containing C. The result would be decreased selectivity when patterning.

When first proposed, third generation synchrotron sources promised bright tunable X-rays which could be used for site-selective fragmentation of molecules (Attwood et al. 1985). There are now numerous literature examples of site-selective fragmentation of predominantly *gas* phase molecules using tunable X-rays (Nenner et al. 1996; Miron et al. 1998). However, Wang et al. (2007a, b) showed that differing X-ray absorption cross-sections and a monochromatic beam are not sufficient to realize this concept in the *condensed* phase. For polymers, it only succeeded when applied to vertically segregated multilayer structures, rather than multiple chemical functional groups sharing the same polymer backbone, or within the monomeric repeat unit. The mechanism put forth by Wang et al. (2007a) to explain the success of the layered structure has since been proven incorrect by Leontowich and Hitchcock (2011) and a new mechanism to explain why patterning is only successful for layered samples is proposed here: the initial core excitation can be made specific by tuning the patterning photon energy to an absorption resonance exclusive to one component. When one component is selectively absorbing X-rays, a cascade of damaging secondary processes is initiated, the dominant process being generation of secondary electrons (photoelectrons, Auger, shake-off, shake-up, etc.). These secondary processes are not specific, and therefore the specificity of the initial core excitation is lost in the condensed phase if both components are within the damaging radius of the secondary processes. However, in a layered sample, there can be sufficient spatial separation of the absorbing and non-absorbing components if enough of the non-resonant layer lies beyond the damaging radius of the secondary processes emitted by the resonant layer, which typically have a range of a few nanometres at soft X-ray photon energies (Seah and Dench 1979). This distance sets a minimum layer thickness for which chemically selective patterning will succeed, which we estimate to be 20 nm for the energy region covered by soft X-ray STXMs. At the other extreme, absorption saturation sets a maximum sample thickness limit; when working at C 1s edge photon energies, the total thickness of all the layered components can only be about 300 nm.

2.1.2 Added requirements for chemically selective lithography

A development step, which often consists of dipping the sample in a suitable solvent to reveal the patterned areas is necessary to realize nanofluidic channels or other unique structures, and differentiates chemically selective patterning (Wang et al. 2007a, b) from the present approach of chemically selective lithography. The solubility of the components of the multilayer sample in the developer must be taken into consideration. If, for example, a bilayer is made of two components which both act as positive resists (irradiated material is removed by developer, non-irradiated material is unaffected), then the developer for the top layer cannot significantly attack/dissolve the non-irradiated portions of the bottom layer and vice versa or the structure would be ruined. With more layers of different components it becomes increasingly difficult to find components with both the appropriate X-ray absorption properties and suitable orthogonal developers.

2.2 Sample preparation

The samples used in this work consist of a 30–100 nm layer of poly(dimethylglutarimide) (PMGI, MicroChem Corp.), on a 30–100 nm layer of poly(methyl methacrylate) (PMMA, electronics grade, $M_w = 315{,}000$ g/mol, $M_w/M_n = 1.05$, Polymer Source Inc.), on a silicon nitride window (nominally Si_3N_4, 75 nm × 1 mm × 1 mm window area in a 200 μm × 5 mm × 5 mm Si frame, Norcada Inc.). PMMA layers were fabricated by spin casting 1.0–2.0 % w/w solutions of PMMA in toluene (99.9 % Chromasolv®, Sigma-Aldrich) onto freshly cleaved mica (Ted Pella Inc.). The layer on mica was scribed into 3 mm × 3 mm pieces with a scalpel, and slowly dipped into a Petri dish of distilled water. Pieces of the film detach from the mica and float on the waters surface, and one piece was then caught on a Si_3N_4 window in an orientation which partially covered the window to allow for subsequent measurements of the spectrum of incident radiation. The sample was then annealed for 1 h at 150 °C at reduced pressure (2×10^{-2} Torr). Next, layers of PMGI were fabricated by spin casting 1.0–2.0 % w/w solutions of PMGI in *N*,*N*-dimethylformamide (99.9 % Chromasolv®, Sigma-Aldrich) onto freshly cleaved mica. The PMGI layer on mica was then annealed for 5 min at 230 °C. One 3 mm × 3 mm piece of PMGI was transferred onto the sample by the float method (described above) in an orientation that partially covered the PMMA layer yet only partially covered the window. This multiple float procedure has opened up greater possibilities for samples than the previous multiple spin casting approach (Wang et al. 2007a, b). Finally, the sample was annealed for 15 min at 150 °C, 2×10^{-2} Torr.

2.3 Scanning transmission X-ray microscope (STXM)

Patterning of samples, collection of near-edge X-ray absorption fine structure (NEXAFS) spectra and imaging was performed with the STXM (Kilcoyne et al. 2003) at beamline 5.3.2.2 (Warwick et al. 2002) at the ALS, Lawrence Berkeley National Laboratories (LBNL, Berkeley, CA, USA). The Fresnel zone plate lens (Howells et al. 2007) supplied by the Center for X-ray Optics had the following parameters: 25 nm outer most zone width, 240 μm diameter, 90 μm central stop. A 50 μm order sorting aperture was used to suppress zero order (un-diffracted) light and a 1.0 m differentially pumped section of beamline filled with 600 mTorr of N_2 was used to suppress beamline second order light. Experiments were performed with the STXM chamber backfilled with 250 Torr He, after the evacuation of air. Entrance (50 μm) and exit (25 μm × 25 μm) slit settings were chosen so that focusing performance would be diffraction-limited, offering the smallest possible spot size (Attwood 1999; Howells et al. 2007). Details of the pattern-generation program and the calculation of doses, which are believed to be accurate and precise within 10 %, have been previously reported elsewhere (Leontowich et al. 2012).

2.4 Development

A 7:3 v/v 2-propanol (IPA, 99.5 %, Caledon Laboratories Ltd.):H_2O solution was used as the developer for PMGI (Johnstone et al. 2008), while a 3:1 v/v IPA:4-methyl-2-pentanone (MIBK, >98.5 % ACS reagent grade, Sigma-Aldrich) solution was used to develop the PMMA layer (Greeneich 1975). The 7:3 IPA:H_2O solution has also been shown to be a developer for PMMA (Yasin et al. 2001). The performance of both developer/resist systems for this application has been explored previously (Leontowich and Hitchcock 2011). The sample was held with locking tweezers, then fully immersed in the PMGI developer and gently stirred for 10 s. The sample was then immediately immersed into the PMMA developer and stirred for 30 s. Afterward, the sample was allowed to dry in ambient air. All development occurred at about 20 °C. These specific development conditions were applied for all results presented in this report.

2.5 Imaging

The nanofluidic structures were imaged by four techniques: optical microscopy (Olympus BX51), atomic force microscopy (AFM, Quesant Q-Scope 350 microscope, Budget Sensors Tap150Al-G probes, intermittent contact mode), NEXAFS spectromicroscopy, and scanning electron microscopy (SEM, JEOL JSM-7000F microscope, 10 keV, 1.4 nA beam current, working distance: 5 mm). A

5 ± 1 nm Pt layer was applied (682 Precision Etching Coating System, Gatan Inc.) prior to SEM imaging to reduce charging and improve contrast. It is imperative to image the structures in the proper order to avoid introducing artefacts. Both SEM and STXM involve ionizing radiation, which can induce mass loss, chemical changes and carbon contamination (Leontowich and Hitchcock 2012b), permanently altering the sample (Coffey et al. 2002; Wang et al. 2009a, b). Optical and AFM imaging did not noticeably alter the sample and therefore were always performed before SEM or STXM imaging. Identical duplicate structures were made on separate samples to obtain artefact-free SEM and STXM images of the same structure.

3 Results

3.1 Layered structure and NEXAFS spectra

An optical micrograph of a PMGI/PMMA/Si_3N_4 sample is presented in Fig. 1a. C 1s NEXAFS spectra were collected from areas of this sample composed of only one of the layers. The optical density scales of these spectra were normalized to correspond to the response for 1 nm thickness of material using the elemental response for the formula repeat units (Henke et al. 1993) and the known bulk densities. These normalized spectra are presented in Fig. 1b. The spectrum of PMGI is dominated by the C 1s(C=O) → $\pi^*_{C=O}$ absorption feature at 287.70 eV, while the spectrum of PMMA is dominated by a slightly larger C 1s(C=O) → $\pi^*_{C=O}$ absorption feature at 288.45 eV. The $\pi^*_{C=O}$ resonance of PMGI is red shifted by 0.75 eV relative to PMMA due to differences in the electronic environment surrounding the carbonyl bond (Urquhart and Ade 2002).

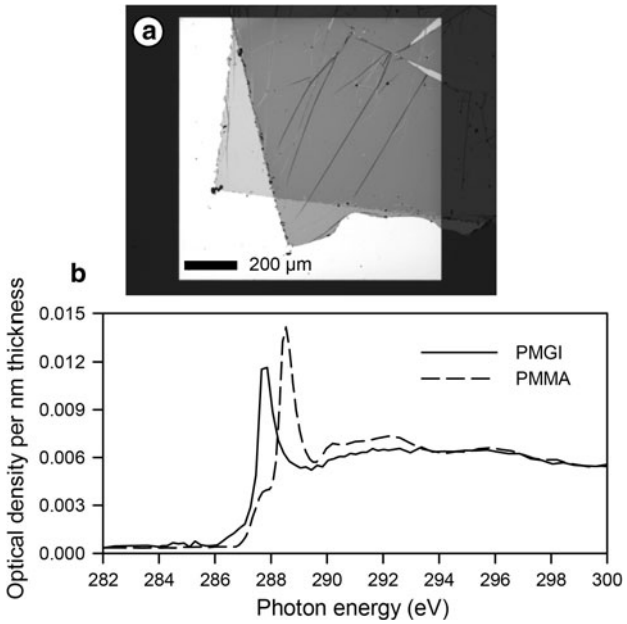

Fig. 1 **a** Optical micrograph (×1.25, transmission) of a PMGI/PMMA bilayer on a Si_3N_4 window. **b** X-ray absorption (NEXAFS) spectra of PMGI and PMMA, normalized to 1 nm thickness

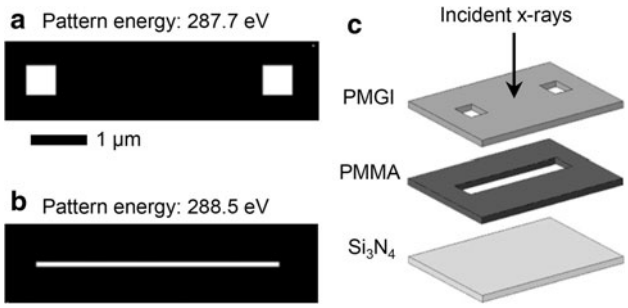

Fig. 2 **a** Pattern A; "access hole" pattern for the top PMGI layer. **b** Pattern B; channel pattern for the bottom PMMA layer. **a**, **b** are on the same spatial scale. **c** Exploded view schematic of the desired nanofluidic structure

3.2 Fabricating nanochannels

Two pattern-generation files, each consisting of sets of discrete points on a 30 nm rectilinear grid, were created to fabricate nanochannels. Pattern A (Fig. 2a) consisted of two parallel 570 nm × 570 nm square areas (i.e., 19 × 19 point exposures) separated by 4,000 nm, while pattern B (Fig. 2b) consisted of a 4,680-nm long, 90-nm wide area. A graphical representation of the final desired structure and its orientation relative to the incident X-ray beam is presented in Fig. 2c. A region of the PMGI/PMMA bilayer was then brought into sharp focus in the STXM and was subsequently chemically selectively patterned in the following manner: the photon energy was set to 287.7 eV and pattern A was executed using the PatternGen routine (Leontowich et al. 2012) in the STXM_Control program with precise dwell time and sample position control [better than 10 nm peak-to-valley by laser interferometry (Kilcoyne et al. 2003)]. After completion, the photon energy was set to 288.5 eV and pattern B was executed over the exact same area as pattern A. Several combined A B patterns were made on the same sample covering a range of dwell times. The sample was then removed from the STXM chamber and developed (Sect. 2.4). The developed samples were loaded into the STXM chamber and imaged at 288.5 eV (Fig. 3). Figure 3a–e is STXM optical density (OD) image of developed patterns generated with successively increasing exposure times (2–5 ms) corresponding to increasing doses (1–3 MGy) for pattern B, while the exposure times for pattern A were held constant (14 ms, 10 MGy).

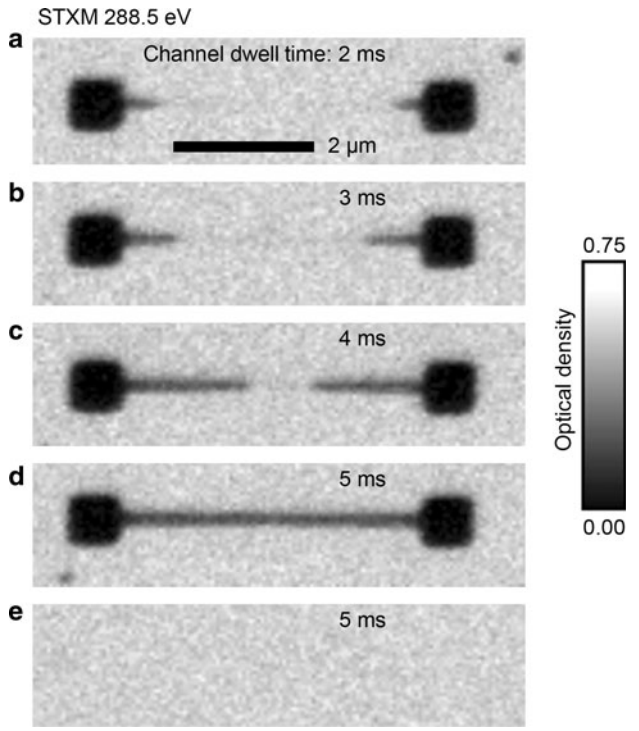

Fig. 3 STXM OD images at 288.5 eV of developed PMGI/PMMA/Si_3N_4 samples patterned with different exposure times for the channel (**a** = 2 ms, **b** = 3 ms, **c** = 4 ms, **d** = 5 ms, **e** = 5 ms). Exposure time for the access holes for **a**–**d** was 14 ms. Access holes were not patterned for **e**. All images are on the same spatial and OD scale

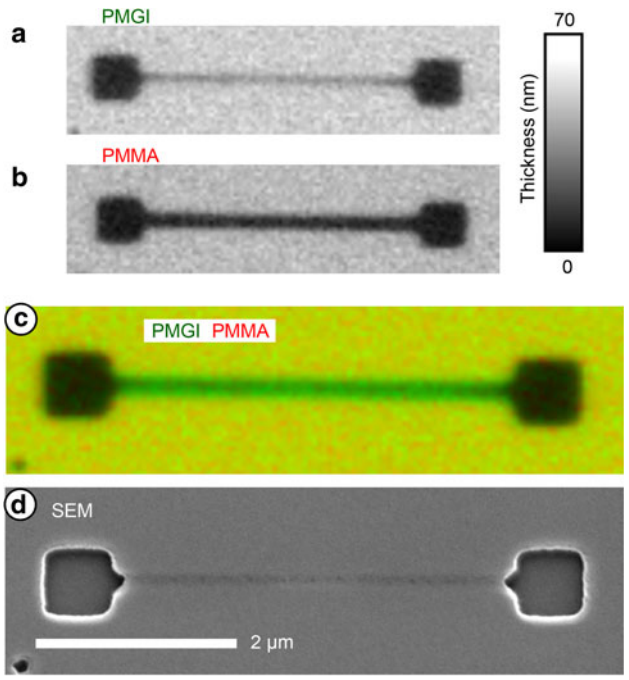

Fig. 4 Quantitative component maps of **a** PMGI and **b** PMMA derived from SVD analysis of a C 1s image sequence on the same positional and thickness scales. **c** Non-rescaled two-color composite map with PMGI in *green*, and PMMA in *red* (color online). *Yellow* corresponds to the presence of both polymer layers (*red* + *green*). **d** Scanning electron micrograph of the nanochannel structure on the same positional scale

The patterned PMMA material in the nanochannel was removed beginning from the square areas of pattern A (i.e., "access holes") inward. As the dose received by the PMMA in the nanochannel area increased, the nanochannel was developed further underneath the PMGI layer. The dose received by the patterned PMMA material in the nanochannel in Fig. 3d was enough that it was fully cleared during development. In Fig. 3e, pattern B was executed with the same dwell time/dose as Fig. 3d, but here pattern A was not executed; the channel received the dose necessary to be cleared, yet in this case the patterned material in the nanochannel was not removed during development.

3.3 Characterization of the nanochannel

A C 1s image sequence, or "stack" (Jacobsen et al. 2000), of the nanochannel structure of Fig. 3d was collected with the STXM. The stack, which consists of a C 1s NEXAFS spectrum for every pixel in the imaged area, was fit to the 1 nm normalized PMGI and PMMA reference spectra (Fig. 1b) using singular value decomposition (SVD) routines (Ade and Hitchcock 2008) implemented in the data analysis program aXis2000 (Hitchcock 2013). The pixel dwell time was kept low (2–4 ms) to minimize radiation damage. Also, the same acquisition parameters (pixel spacing, dwell time, photon energy region and number of energy points) were used to collect this stack and the reference spectra to cancel out damage artefacts before the SVD fit. Figure 4 displays the resulting PMGI (Fig. 4a) and PMMA (Fig. 4b) component maps along with a color-coded composite (Fig. 4c). Because the NEXAFS reference spectra used in the fit procedure were normalized to 1 nm material, the component maps are *quantitative*—the intensity scale gives the thickness (in nanometres) of each component in the system. There are only two components in this system (PMGI and PMMA). The fit is very good and allows an accurate (±5 %) determination of the thickness of each layer at every pixel. The total thickness of the bilayer derived from the individual component maps is consistent with data from an atomic force micrograph of the structure (not shown) within measurement uncertainties. The thickness of the PMMA layer within the nanochannel area is equal to that of the developed access hole areas based on SVD analysis of the C 1s NEXAFS spectrum of the nanochannel. This indicates that the patterned PMMA in the nanochannel area has been fully removed by the developer. The thickness of the PMGI layer in the area of the nanochannel, which serves to seal it, is slightly different from elsewhere on the sample; there was loss of 20 % of the PMGI top layer in the patterned nanochannel

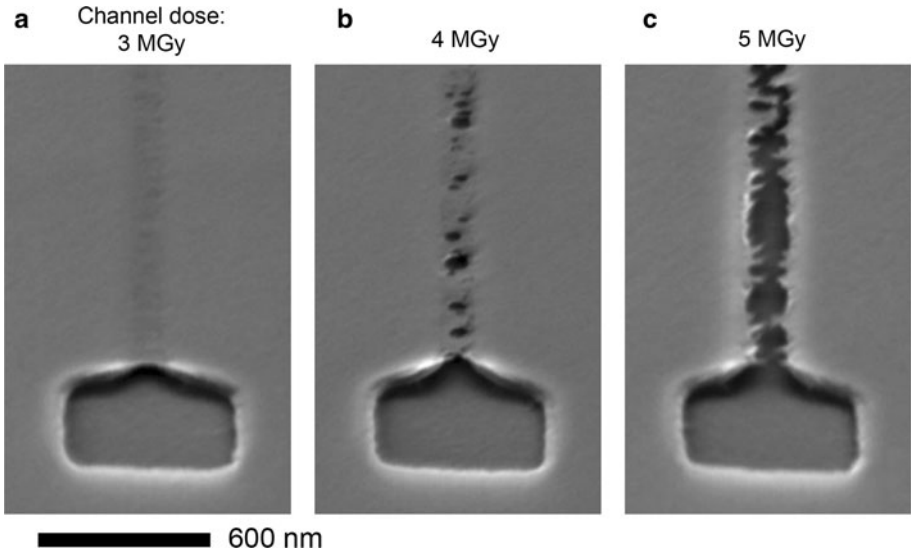

Fig. 5 Scanning electron micrographs of nanochannels collected at a 45° view angle fabricated by chemically selective lithography. **a** Under optimal dose conditions (3 MGy), the channel was cleared and the PMGI overlayer remained intact. **b** Pinholes appeared at channel doses >3.5 MGy, or **c** the PMGI overlayer was fully removed. All images are on the same spatial scale

area. A scanning electron micrograph was also taken of the nanochannel structure of Fig. 3d and is presented in Fig. 4d. The morphology of the square areas is consistent with that of bare Si_3N_4, and despite some loss of PMGI the layer sealing the nanochannel appears intact and free of pinholes.

3.4 Optimizing doses and development times

Scanning electron micrographs of developed nanochannel structures collected at a 45° view angle are presented in Fig. 5. The dwell time/dose to the channel in Fig. 5a was the same as Fig. 3d. The entrance to the nanochannel is clearly observed, as well as the defect-free PMGI top layer. Scanning electron micrographs of nanochannel structures fabricated with increased doses are presented in Fig. 5b, c. Pinhole defects in the PMGI top layer were observed as the dose was increased and eventually this covering layer was fully removed. Thus under the conditions presented, a "dose window" between 2.5 and 3.5 MGy exists in which the patterned PMMA in the nanochannel can be fully cleared while the top PMGI remains free of pinhole defects, sealing the channel.

The development time for both PMGI and PMMA developers was optimized. To reduce the removal of the PMGI layer sealing the nanochannel, the amount of time the sample spends in PMGI developer should be as short as possible. It was found that the development time could be reduced to 10 s if the dwell time for pattern A was increased. This was acceptable as both layers in the patterned area (access holes) need to be fully removed to the substrate, although a larger increase in dwell time will result in rounded edges and expanded holes (Sect. 4.3). It is also conceivable that the amount of time the sample spends in PMMA developer should be as long as possible to increase the maximum nanochannel length. PMMA development times of 30, 60 and 120 s were tested, but it was found that 60 and 120 s only increased the number and size of pinholes in the PMGI layer covering the nanochannel, therefore 30 s was optimal.

3.5 Cross-sectional area of the nanochannel in relation to its maximum length

The pattern-generation files were modified to explore the effect of a wider patterned channel area on the developed length. One 570 nm × 570 nm square was deleted from pattern A. The length of pattern B was increased to 30 μm while the width was varied (60, 90, 150, and 210 nm). Patterning of the sample was carried out as previously described. The dwell time per pixel was constant for all modified pattern B channel patterns (5 ms), as well as the modified pattern A (14 ms). The patterned samples were then developed and imaged using STXM and AFM (Fig. 6).

The STXM OD images show that as the width of the patterned nanochannel was increased, its developed length increased. Atomic force micrographs reveal the entire nanochannel area pattern underwent a decrease in height. A cross comparison with the STXM OD images reveals that this height reduction was the same whether the patterned PMMA material underneath was removed or not. This result suggests that the height reduction is due to removal of PMGI during development, rather than "sagging" of the PMGI top layer over the nanochannel, which is in agreement with the PMGI component map (Fig. 4a).

Although the same dwell times were used for all nanochannel patterns (pattern B) in Fig. 6, the dose for the

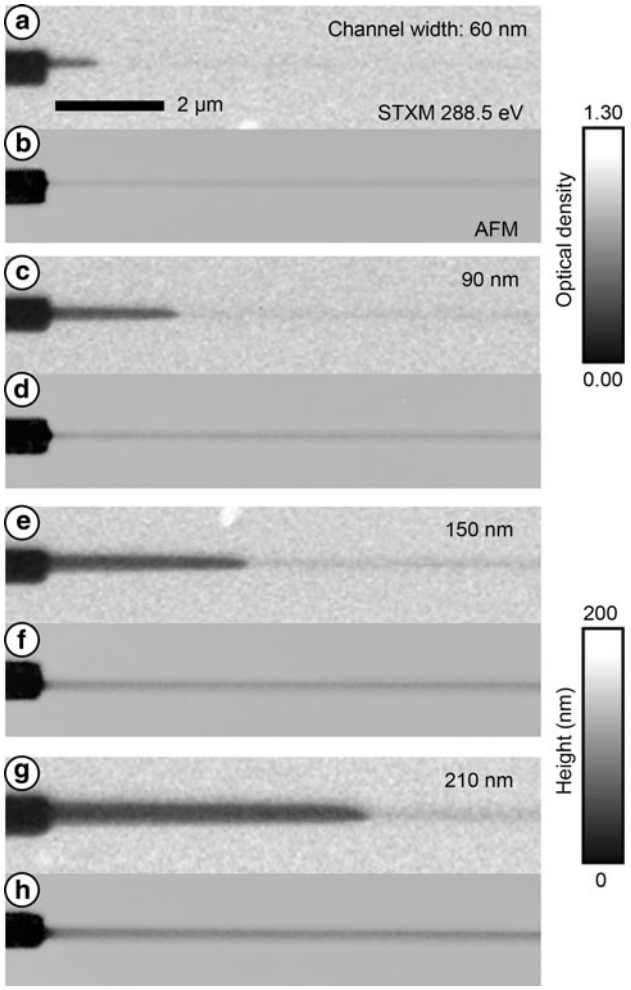

Fig. 6 STXM OD images at 288.5 eV (**a**, **c**, **e**, **g**) and atomic force micrographs (**b**, **d**, **f**, **h**) of nanochannels created with the same dwell time (5 ms) but different widths (60, 90, 150 and 210 nm, respectively). STXM and AFM images are on the same OD and z scale, respectively, and all images are on the same spatial scale

wider channels is not precisely the same as that of the narrower channels. The intense spot of focused X-rays at the focal plane is a distribution [often showing side lobes (Leontowich et al. 2011), characteristics of being diffraction-limited] rather than a finite circle, thus there is a cumulative dose overlap from adjacent exposures and as a result the material at the center of the channel receives a higher dose than that at the edges. However, a conceptually analogous experiment yielded an identical result: the height of the nanochannel is dependent upon the thickness of the bottom layer, which can be fine-tuned by adjusting the concentration of polymer solution before spin casting; increasing the thickness of the bottom PMMA layer effectively increases the cross-sectional area of the nanochannel. With a 40 nm layer of PMMA, the maximum length that a 90-nm-wide nanochannel could be fully cleared yet free of pinholes was 5 ± 1 μm. This distance increased to 8 ± 1 μm with a 90 nm layer of PMMA.

4 Discussion

4.1 Maximum nanochannel length

Patterning of the nanochannel was performed at 288.5 eV which is very near the maximum absorption cross-section of PMMA at the C 1s edge. The energy absorption rate of PMMA at this photon energy is significantly greater than that of PMGI allowing selective patterning in the PMMA layer. However, PMGI also absorbs energy, albeit at a lower rate, because the absorption cross-section of PMGI at 288.5 eV is not zero (Fig. 1b). This residual dose into the PMGI top layer while patterning the nanochannel is enough to cause partial removal of the PMGI top layer, which was observed by NEXAFS spectromicroscopy (Fig. 4a) and AFM (Fig. 6). Within an experimentally determined dose window, this process is insignificant overall as PMGI remains continuous and seals the nanochannel. But at higher dwell times the residual dose induces significant pinhole formation and eventually results in the full removal of the PMGI layer. This imposes an upper limit on the dwell time for patterning the nanochannel, even when performed chemically selectively.

To realize the nanochannel, the PMMA developer solution must diffuse under the PMGI layer, into the nanochannel, dissolve the patterned PMMA material, and then diffuse out. When PMMA is exposed to ionizing radiation at low dose, it primarily undergoes main chain scission which decreases the molecular weight and dramatically increases solubility in the PMMA developer (Greeneich 1975). The development/excavation process of the patterned PMMA material in the nanochannel can therefore be facilitated by increasing the dose to the nanochannel, but only up to the limit imposed by pinhole formation in the PMGI layer. The maximum length of the channel then becomes dependent upon the diffusion of developer into and out of the nanochannel. The longer the channel is, the more difficult excavating the patterned material inside the channel becomes. The diffusion-limited excavation can be aided by increasing the cross-sectional area of the nanochannel; conceivably better flow occurs. Previous reports involving excavation of positive mode channels with transverse dimensions in the micrometre range did not report such issues (Zhou et al. 2002; Gansel et al. 2009). However, this deviates from the uniqueness of this approach as the nanochannels take on larger dimensions. The maximum length that a 100 nm × 100 nm nanochannel could be fabricated without pinholes was 10 ± 1 μm.

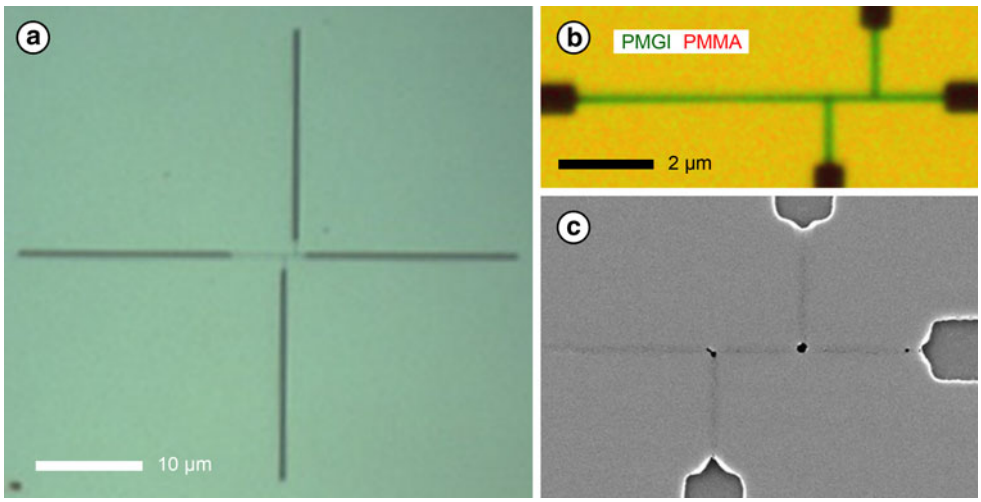

Fig. 7 A double T injector device fabricated by chemically selective lithography. **a** Optical micrograph (×100, reflection) of the entire device. **b** Non-rescaled two-color composite map (PMGI in *green*, PMMA in *red*, color online) derived from SVD analysis of a C 1s image sequence recorded with STXM. **c** Scanning electron micrograph of the device

4.2 Interfacing with conventional microfluidics

The nanochannels fabricated here appear to be tightly sealed and should be viable working fluidic devices. The impermeability of the PMGI overlayer sealing the nanochannel is demonstrated in Fig. 3e. In this example, only pattern B was carried out at the dose required to clear the nanochannel. Without defined access holes, either the developer could not reach the patterned PMMA or the solvated material could not escape (or a combination of these two effects) and the nanochannel was not realized. Work on functioning fluidic devices has begun. Images of a double T injector test structure fabricated with STXM 5.3.2.2 are presented in Fig. 7. A challenge now is plumbing this device so that the flow of liquid in and out can be controlled, and the flow rate measured, etc. Attempts are currently being made towards interfacing this structure with more conventional microchannels by bonding a poly(dimethylsiloxane) chip on top of the structure (McDonald and Whitesides 2002). To that end, the access holes have been extended to a length of 50 µm to ease the alignment constraints when mating the two structures.

4.3 Outlook

For a functional nanofluidic device the components of the structure must ultimately be compatible with the solvent and analyte molecules. The PMGI/PMMA/Si_3N_4 nanochannels described here are stable in distilled water for at least 24 h. Here, the X-ray absorption cross-sections of the two components were just different enough to be viable, but it would be beneficial if the difference was much larger. Furthermore, the orthogonal developer requirement imposes limits which hinder further evolution to completely three-dimensional fluidic systems. Perhaps a better approach would be to use one resist with different initiator molecules such as photoacid generators (Pawloski et al. 2002) in layers which would bypass the need for an orthogonal developer for each layer. Use of self-developing resists (Ito and Wilson 1983) would alleviate both the orthogonal developer and diffusion issues. Moving to higher X-ray photon energies may allow patterning and fabrication of thicker, more complex structures as photoabsorption cross-sections decrease with increasing photon energy, reducing absorption saturation. However, the damaging radii of secondary processes increases; the inelastic mean free path increases with higher photon energies beyond the C 1s edge (Seah and Dench 1979). Therefore, the soft X-ray region appears best suited to this type of approach.

Direct write patterning using STXM would benefit from a point-spread function (Leontowich et al. 2011) correction program which would calculate the cumulative dose overlap from adjacent exposures and adjust the dwell time for each pixel to correct for it. For example, the holes seen only at the nexus of several nanochannels (Fig. 7c) are likely due to overlap of point-spread functions. Solutions to this problem exist for electron beam lithography (Pavkovich 1986), but have yet to be applied to patterning using STXM. Finally, the concept of chemically selective lithography (Sect. 2.1) demonstrated here is not exclusive to direct write geometry, which is serial and not well suited to mass production of devices. There is a clear path to parallel mass production using multiple patterned masks, one for each layer/photon energy exposed to a collimated monochromatic beam. The multiple mask exposures would need to be precisely aligned, but this technology is already established within the X-ray lithography community (Schmidt et al. 1996). Chemically selective lithography requires tunable soft X-rays. Therefore, the experiment would require mating an X-ray lithography scanner endstation with multiple patterning ability to a monochromated

soft X-ray beamline at a synchrotron facility, a tunable energy laser (Popmintchev et al. 2012), or a tunable plasma X-ray source (Labate et al. 2002).

5 Conclusions

Sealed nanochannels with sub-100 nm dimensions were created in polymer bilayers with tunable focused soft X-rays in direct write geometry. For a 100 nm × 100 nm cross-section, the maximum nanochannel length realized was 10 ± 1 μm. Excavation of the patterned channel material was found to be the largest impediment to the realization of even longer channels. Longer channels can be realized if the cross-sectional area is increased.

Acknowledgments This research was supported by the Natural Sciences and Engineering Research Council of Canada, the Canada Foundation for Innovation and the Canada Research Chair program. We thank Dongqing Li and Jose Moran-Mirabal for useful discussion on interfacing microfluidics with nanofluidics, Yujie Zhu for performing initial interfacing experiments, and Ash Parameswaran for providing the poly(dimethylglutarimide). We also thank David Kilcoyne and Tolek Tyliszczak for their support of the STXM facilities. The experiments were performed at beamline 5.3.2.2 of the ALS, LBNL. The ALS is supported by the Director, Office of Energy Research, Office of Basic Energy Sciences, Materials Sciences Division of the USA Department of Energy, under Contract No. DE-AC03-76SF00098. A.F.G.L. acknowledges support from an ALS doctoral fellowship in residence.

References

Ade H, Hitchcock AP (2008) NEXAFS microscopy and resonant scattering: composition and orientation probed in real and reciprocal space. Polymer 49:643–675. doi:10.1016/j.polymer.2007.10.030

Attwood D (1999) Soft X-rays and extreme ultraviolet radiation: principles and applications. Cambridge University Press, Cambridge

Attwood D, Halbach K, Kim KJ (1985) Tunable coherent X-rays. Science 228:1265–1272. doi:10.1126/science.228.4705.1265

Coffey T, Urquhart SG, Ade H (2002) Characterization of the effects of soft X-ray irradiation on polymers. J Elec Spec Relat Phenom 122:65–78. doi:10.1016/S0368-2048(01)00342-5

Fouad M, Yavuz M, Cui B (2010) Nanofluidic channels fabricated by e-beam lithography and polymer reflow sealing. J Vac Sci Technol B 28:C6I11–C6I13. doi:10.1116/1.3517620

Gansel JK, Thiel M, Rill MS, Decker M, Bade K, Saile V, Freymann GV, Linden S, Wegener M (2009) Gold helix photonic metamaterial as broadband circular polarizer. Science 325:1513–1515. doi:10.1126/science.1177031

Greeneich JS (1975) Developer characteristics of poly-(methyl methacrylate) electron resist. J Electrochem Soc 122:970–976. doi:10.1149/1.2134380

Henke BL, Gullikson EM, Davis JC (1993) X-ray interactions: photoabsorption, scattering, transmission, and reflection at E = 50–30,000 eV, Z = 1–92. Atom Data Nucl Data Tables 54:181–342. doi:10.1006/adnd.1993.1013

Hitchcock AP (2013) aXis2000 is written in interactive data language (IDL). It is available free for non-commercial use. http://unicorn.mcmaster.ca/aXis2000.html

Howells M, Jacobsen C, Warwick T (2007) Principles and applications of zone plate X-ray microscopes. In: Hawkes PW, Spence JCH (eds) Science of microscopy, vol 2. New York, Springer Science + Business Media, pp 835–926. doi:10.1007/978-0-387-49762-4_13

Ito H, Wilson CG (1983) Chemical amplification in the design of dry developing resist materials. Polym Eng Sci 23:1012–1018. doi:10.1002/pen.760231807

Jacobsen C, Wirick S, Flynn G, Zimba C (2000) Soft X-ray spectroscopy from image sequences with sub-100 nm spatial resolution. J Microscopy 197:173–184. doi:10.1046/j.1365-2818.2000.00640.x

Johnstone RW, Foulds IG, Pallapa MV, Parameswaran AM (2008) Isopropanol/water as a developer for poly(dimethylglutarimide). J Micro/Nanolith MEMS MOEMS 7:043006. doi:10.1117/1.2990738

Kilcoyne ALD, Tyliszczak T, Steele WF, Fakra S, Hitchcock P, Franck K, Anderson E, Harteneck B, Rightor EG, Mitchell GE, Hitchcock AP, Yang L, Warwick T, Ade H (2003) Interferometer-controlled scanning transmission X-ray microscopes at the Advanced Light Source. J Synchrotron Rad 10:125–136. doi:10.1107/S0909049502017739

Labate L, Galimberti M, Giulietti A, Giulietti D, Gizzi LA, Tomassini P, Di Cocco G (2002) A laser-plasma source for CCD calibration in the soft X-ray range. Nucl Instrum Meth A 495:148–153. doi:10.1016/S0168-9002(02)01573-5

Leontowich AFG, Hitchcock AP (2011) Zone plate focused soft X-ray lithography. Appl Phys A 103:1–11. doi:10.1007/s00339-010-6172-4

Leontowich AFG, Hitchcock AP (2012a) Zone plate focused soft X-ray lithography for fabrication of nanofluidic devices. Proc SPIE 8323:83231D. doi:10.1117/12.915803

Leontowich AFG, Hitchcock AP (2012b) Secondary electron deposition mechanism of carbon contamination. J Vac Sci Technol B 30:030601. doi:10.1116/1.3698602

Leontowich AFG, Tyliszczak T, Hitchcock AP (2011) Measurement of the point spread function of a soft X-ray microscope by single pixel exposure of photoresists. Proc SPIE 8077:80770N. doi:10.1117/12.887553

Leontowich AFG, Hitchcock AP, Tyliszczak T, Weigand M, Wang J, Karunakaran C (2012) Accurate dosimetry in scanning transmission X-ray microscopes via the cross-linking threshold dose of poly(methyl methacrylate). J Synchrotron Rad 19:976–987. doi:10.1107/S0909049512034486

Leontowich AFG, Hitchcock AP, Watts B, Raabe J (2013) Sub-25 nm direct write (maskless) x-ray nanolithography. Microelec Eng. doi:10.1016/j.mee.2013.03.006

McDonald JC, Whitesides GM (2002) Poly(dimethylsiloxane) as a material for fabricating microfluidic devices. Acc Chem Res 35:491–499. doi:10.1021/ar010110q

Miron C, Simon M, Leclercq N, Hansen DL, Morin P (1998) Site-selective photochemistry of core excited molecules: role of the internal energy. Phys Rev Lett 81:4104–4107. doi:10.1103/PhysRevLett.81.4104

Nenner I, Reynaud C, Schmelz HC, Ferrand-Tanaka L, Simon M, Morin P (1996) Site selective fragmentation with soft X-rays: from gaseous polyatomic molecules, free clusters, polymers, adsorbates to biological macromolecules. Z Phys Chem 195:43–63. doi:10.1524/zpch.1996.195.Part_1_2.043

Park S, Huh YS, Craighead HG, Erickson D (2009) A method for nanofluidic device prototyping using elastomeric collapse. PNAS 106:15549–15554. doi:10.1073/pnas.0904004106

Pavkovich JM (1986) Proximity effect correction calculations by the integral equation approximate solution method. J Vac Sci Technol B 4:159–163. doi:10.1116/1.583369

Pawloski AR, Nealey PF, Conley W (2002) Efficiency of photoacid generators in chemically amplified resists for 157 nm lithography. J Photopolymer Sci Tech 15:731–739. doi:10.2494/photopolymer.15.731

Popmintchev T, Chen MC, Popmintchev D, Arpin P, Brown S, Ališauskas S, Andriukaitis G, Balčiunas T, Mücke OD, Pugzlys A, Baltuška A, Shim B, Schrauth SE, Gaeta A, Hernández-García C, Plaja L, Becker A, Jaron-Becker A, Murnane MM, Kapteyn HC (2012) Bright coherent ultrahigh harmonics in the keV X-ray regime from mid-infrared femtosecond lasers. Science 336:1287–1291. doi:10.1126/science.1218497

Schmidt A, Ehrfeld W, Lehr H, Müller L, Reuther F, Schmidt M, Zetterer Th (1996) Aligned double exposure in deep X-ray lithography. Microelec Eng 30:235–238. doi:10.1016/0167-9317(95)00235-9

Seah MP, Dench WA (1979) Quantitative electron spectroscopy of surfaces: a standard data base for electron inelastic mean free paths in solids. Surf Interface Anal 1:2–11. doi:10.1002/sia.740010103

Stavis SM, Edel JB, Samiee KT, Craighead HG (2005) Single molecule studies of quantum dot conjugates in a submicrometer fluidic channel. Lab Chip 5:337–343. doi:10.1039/b416161k

Urquhart SG, Ade H (2002) Trends in the carbonyl core (C 1s, O 1s) $\rightarrow \pi^*_{C=O}$ transition in the near-edge X-ray absorption fine structure spectra of organic molecules. J Phys Chem B 106:8531–8538. doi:10.1021/jp0255379

Wang J, Stöver HDH, Hitchcock AP, Tyliszczak T (2007a) Chemically selective soft X-ray patterning of polymers. J Synchrotron Rad 14:181–190. doi:10.1107/S0909049506053829

Wang J, Stöver HDH, Hitchcock AP (2007b) Chemically selective soft X-ray direct-write patterning of multilayer polymer films. J Phys Chem C 111:16330–16338. doi:10.1021/jp072570s

Wang J, Morin C, Li L, Hitchcock AP, Scholl A, Doran A (2009a) Radiation damage in soft X-ray microscopy. J Elec Spec Relat Phenom 170:25–36. doi:10.1016/j.elspec.2008.01.002

Wang J, Botton GA, West MM, Hitchcock AP (2009b) Quantitative evaluation of radiation damage to polyethylene terephthalate by soft X-rays and high-energy electrons. J Phys Chem B 113:1869–1876. doi:10.1021/jp808289e

Warwick T, Ade H, Kilcoyne D, Kritscher M, Tylisczcak T, Fakra S, Hitchcock A, Hitchcock P, Padmore H (2002) A new bend-magnet beamline for scanning transmission x-ray microscopy at the Advanced Light Source. J Synchrotron Rad 9:254–257. doi:10.1107/S0909049502005502

Winston D, Cord BM, Ming B, Bell DC, DiNatale WF, Stern LA, Vladar AE, Postek MT, Mondol MK, Yang JKW, Berggren KK (2009) Scanning-helium-ion-beam lithography with hydrogen silsesquioxane resist. J Vac Sci Technol B 27:2702–2706. doi:10.1116/1.3250204

Yang JKW, Cord B, Duan H, Berggren KK, Klingfus J, Nam S, Kim K, Rooks MJ (2009) Understanding of hydrogen silsesquioxane electron resist for sub-5-nm-half-pitch lithography. J Vac Sci Technol B 27:2622–2627. doi:10.1116/1.3253652

Yasin S, Hasko DG, Ahmed H (2001) Fabrication of <5 nm width lines in poly(methylmethacrylate) resist using a water:isopropyl alcohol developer and ultrasonically-assisted development. Appl Phys Lett 78:2760–2762. doi:10.1063/1.1369615

Zhang X, Jacobsen C, Lindaas S, Williams S (1995) Exposure strategies for polymethyl methacrylate from in situ X-ray absorption near edge structure spectroscopy. J Vac Sci Technol B 13:1477–1483. doi:10.1116/1.588175

Zhou W, Kuebler SM, Braun KL, Yu T, Cammack JK, Ober CK, Perry JW, Marder SR (2002) An efficient two-photon-generated photoacid applied to positive-tone 3D microfabrication. Science 296:1106–1109. doi:10.1126/science.296.5570.1106